Ohmic contact formation mechanisms of TiN film on 4H–SiC

Zhongtao Wang[a,1], Xijun Wang[b,1], Wei Liu[a], Xiaoliang Ji[a], Chunqing Wang[a,c,*]

[a] *State Key Laboratory of Advanced Welding and Joining, Harbin Institute of Technology, Harbin, 150001, People's Republic of China*
[b] *Department of Chemical and Biomolecular Engineering, North Carolina State University, Raleigh, NC, 27606, United States*
[c] *Key Laboratory of Micro-systems and Micro-structures Manufacturing, Ministry of Education, Harbin Institute of Technology, Harbin, 150080, People's Republic of China*

A B S T R A C T

The atomic structure, interfacial charge distribution, bonding nature, and interfacial electronic states of a 4H–SiC/TiN interface are systematically investigated to understand the Ohmic contact formation mechanisms of TiN to 4H–SiC. The experiment results clearly demonstrate that the well-arranged TiN (111)-oriented lattice planes are parallel to the (0001) SiC-oriented substrate, which is in line with the XRD results. In addition, the interface is coherent without any secondary phase layers, amorphous layers, or transition regions, which confirms the direct contact of TiN to SiC at the atomic scale, exhibiting a linear current–voltage relationship. Quantitatively, first-principle calculations reveal that the Schottky barrier height (SBH) is as low as 0.03 eV and that the band gap nearly vanishes at the interface, indicating an excellent Ohmic contact of TiN to 4H–SiC. Furthermore, the SBH is significantly reduced through the interfacial charge polarization effect and strong coupling of interfacial electronic states, enhancing the quantum electron transport. The present results provide insight into the complicated electronic effects of the Ohmic contact interface and indicate that TiN is a promising SiC Ohmic contact material for advanced next-generation power device applications.

1. Introduction

The promising properties of SiC, such as high thermal conductivity, high breakdown voltage, and high-saturation electron drift velocity [1], have stimulated extensive investigations into the fabrication of electronic devices applied in high-frequency, ultra-high voltage, and high-temperature areas [2]. However, a major challenge for integrating SiC is controlling the metal/SiC Ohmic contact properties [3,4]. Over the past few decades, numerous studies have been conducted on Ohmic contacts to SiC, which include Ni [5], Al/Ti [6], Ni/Ti/Al [7], and so on. To date, in most studies the contacts have to anneal at high temperature to obtain better Ohmic contacts performance, and it is therefore difficult to understand the Ohmic contact formation mechanisms owing to severe interfacial reactions and/or inter-diffusion [1]. Different explanations for the origins of Ohmic contacts have been proposed, such as the formation of silicides or carbides [8,9], carbon vacancies [10], interface pinning, and/or spiking [11], etc. Even worse, extremely high temperatures that occur during the Ohmic contact fabrication process may cause thermal stress in the device structures [12], and severe chemical reactions could cause a non-uniformity of the

current distribution, thereby degrading the performance of the Ohmic contacts [5,6]. It is therefore necessary to develop stable contact materials to prohibit the interfacial chemical reaction and solid-state diffusion. Owing to its low work function [13] and good electrical conductivity [14], TiN has been employed as an effective Ohmic contact material with SiC [14,15], exhibiting an excellent thermodynamic stability at up to 1100 °C [16,17]. However, the role of the SiC/TiN interface in the mechanism through which a Schottky barrier becomes Ohmic remains unclear. Glass et al. [18] considered that the Ohmic behavior of TiN to SiC was due to the formation of a thin amorphous interlayer. Lliadis et al. [15] proposed the idea that the surface-modification process played a key role in reducing the effective Schottky barrier height. In addition, to the best of our knowledge, a theoretical understanding of how the Schottky barrier reduction occurs in a SiC/TiN interface has yet to be properly achieved. So, in this work, the interfacial atomic structure of a TiN Ohmic contact to 4H–SiC is systematically studied by combing first-principle calculations with an HRTEM analysis, providing a thorough understanding of the mechanism underlying an Ohmic formation.

* Corresponding author. State Key Laboratory of Advanced Welding and Joining, Harbin Institute of Technology, Harbin, 150001, People's Republic of China.
  E-mail address: wangcq@hit.edu.cn (C. Wang).
[1] Z.W. and X.W. contributed equally to this study.

2. Experiment

The substrates applied were 4° off-axis n-doped 4H–SiC (0001) wafers with a doping concentration of approximately 10^{18} cm^{-3}. First, the substrates were carefully cleaned using a modified RCA solution and dried with nitrogen gas. Then, W(200 nm)/TiN(200 nm)/SiC contacts were fabricated through magnetron sputtering using a designed quartz mask and patterned by applying a lift-off process, as described elsewhere [17]. These structures were then treated with rapid thermal annealing (RTA) at 800 °C for 3 min in an Ar atmosphere. Finally, the Ohmic contact performance was characterized through I–V measurements using a Keithley 4200 source meter unit.

The phase structure of the W/TiN/SiC systems were examined using X-ray diffraction (XRD) with Co Kα radiation. For the interface characterizations, the cross sections of W/TiN/SiC samples were observed using a high-resolution transmission electron microscope (HRTEM) equipped with a high-angle annular dark-field (HADDF) detector in the STEM system. An energy-dispersive X-ray (EDX) analysis across the interface in the STEM system was also conducted. The TEM samples were fabricated using milling samples through a focused ion beam process.

3. Computational details

Calculations of the geometric and electronic structures were conducted using the Vienna ab initio Simulation package [19], employing projector augmented wave pseudopotentials [20] and Perdew-Burke-Ernzerhof (PBE) functions [21]. The kinetic energy cutoff for the planewave basis was set to 400 eV. In addition, the energy and force convergence criteria were set to 10^{-5} eV and 0.01 eV/Å, respectively. A k-point grid with a $7 \times 7 \times 1$ Gamma-centered mesh was employed for the 4H–SiC/TiN slab unit cell. For all supercells, a corresponding number of k-points were employed to maintain the k-mesh spacing constant across different structures. The strong on-site Coulomb interaction on the d-orbital electrons at the Ti-sites was treated using the GGA + U approach [22]. We adopted U_{eff} = 3.5 eV for a Hund's exchange interaction, which has been proven in previous studies to provide reasonable predictions of both geometric and electronic structures [23]. In addition, we used the Bader charge model [24] to analyze the charge distribution at the 4H–SiC/TiN interface.

To build the 4H–SiC/TiN interface model, a 4H–SiC(0001) surface with two types of exposed Si sites (Si1 and Si2) was chosen to combine with a Ti-terminated TiN(111) surface, as shown in Fig. 1. The N-termination was not considered herein because Ti-termination has been

Table 1
Adhesion energy Wad (in J/m^2) for the interfaces between Si-terminated SiC(0001) and TiN (111) terminated with Ti site.

SiC/TiN	Si top	C top	Hollow
Si1 site/TiN	unstable	4.43415	3.98488
Si2 site/TiN	unstable	4.46412	4.08404

proven to be more consistent with the experimental work function for a TiN(111) surface [25]. For each possible combination, the terminated Ti-atoms can sit on three possible site, i.e., Si top, C top, and hollow sites of the 4H–SiC(0001) surface. To determine the most stable interfacial structure, the physically comparable adhesion energy W_{ad} is defined as follows [26]:

$$W_{ad} = (E_{SiC} + E_{TiN} - E_{IF})/A \tag{1}$$

where E_{SiC}, E_{TiN} and E_{IF} are the total energies of the isolated 4H–SiC(0001) slab, TiN(111) slab, and 4H–SiC/TiN interface, respectively, and A is the total interface area. Hence, a larger W_{ad} means a more stable binding of the two slabs.

The calculated adhesion energies are listed in Table 1, in which Si2 of the SiC on-top binding of the Ti site of TiN is determined to be the most stable interfacial configuration for the subsequent calculations.

4. Results and discussion

Fig. 2 shows a typical HADDF-STEM image of the W/TiN/SiC contact system. Evidently, the SiC surface is covered entirely by a uniform TiN film with no cracks or holes. In addition, from Fig. 2b–f, one can see that the substrate is composed of Si and C, and the contact layer is composed of Ti and N. Moreover, no elemental inter-diffusion occurs between the interface of TiN/SiC. To further observe the atomic structure of the interface, a cross-sectional HRTEM image of the SiC/TiN interface is shown in Fig. 3. It can be seen that the well-arranged TiN (111)-oriented lattice fringes are parallel to the (0001) SiC-oriented substrate, which is in line with the XRD patterns (Fig. 4), indicating that TiN exhibits strongly (111)-oriented textures. In addition, these results agree well with the experiment results of Yang et al. [27] and Hultman et al. [14]. Moreover, these orientation relationships are obviously beneficial to forming a well-matched interface between the SiC and TiN because SiC belongs to the hexagonal $P6_3mc$ space group with a = 3.081 Å and c = 10.085 Å, and TiN belongs to the cubic $Fm\bar{3}m$ space group with a = 4.236 Å, which are nearly the same lattice
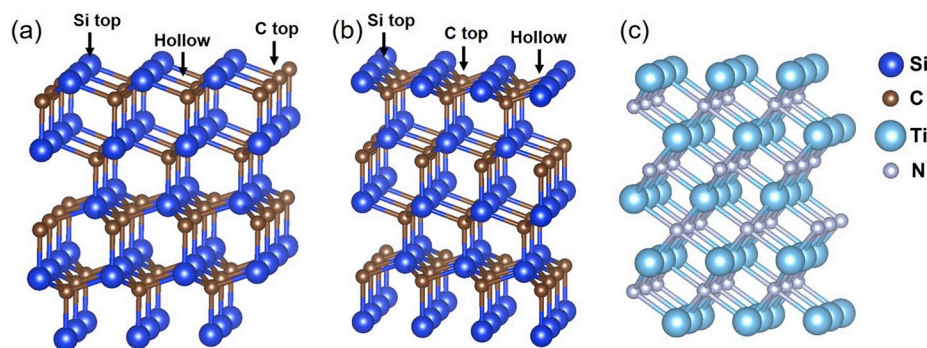
Fig. 1. Atomic structures of 4H–SiC(0001) surface with (a) Si1 and (b) Si2 termination, and TiN(111) surface with (c) Ti termination.
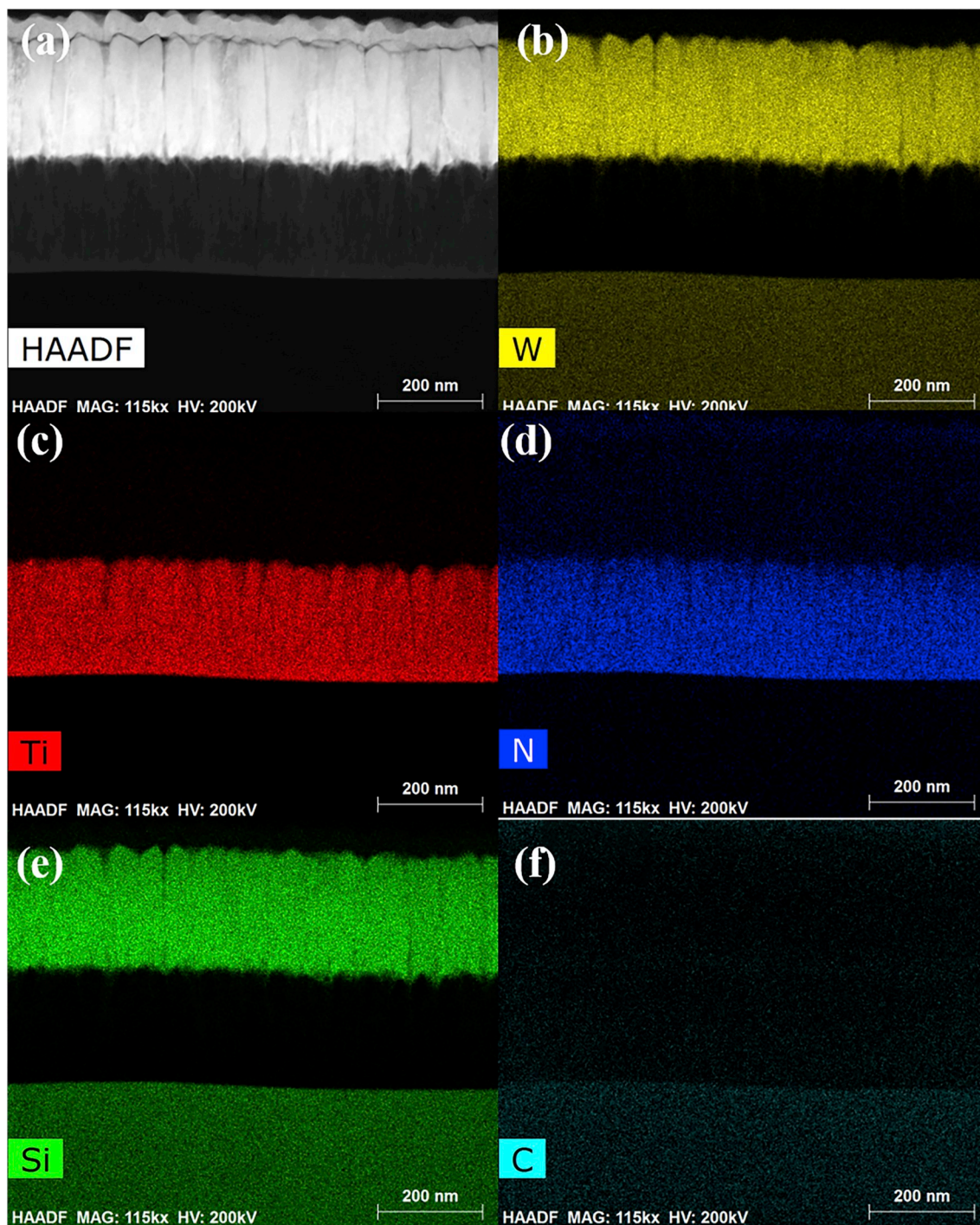
Fig. 2. Cross-sectional HADDF-STEM image of (a) W/TiN/SiC contact and element distributions of (b) W, (c) Ti, (d) N, (e) Si, and (f) C.

constants of the TiN(111) and SiC(0001) lattice planes. Evidently, the interface is coherent without any secondary phase layers, amorphous layers, or transition regions, which confirms the epitaxial growth of TiN films on SiC [27] (Fig. 3b). In addition, this atomic-scale contact should qualitatively be the formation origin of the Ohmic contact of TiN to SiC, as shown in Fig. 5, which shows a linear current–voltage relationship.

To investigate the Ohmic contact mechanism theoretically, first-principle calculations are carried out to study the atomic structure, energetics, and bonding of the TiN/SiC interface. Prior to the simulations of the interfacial structures, we conduct bulk calculations to assess the accuracy of the computational methods. The computed lattice constants of both 4H–SiC (a = b = 3.088 Å, c = 10.109 Å) and TiN (a = b = c = 4.307 Å) agree well with the experiment measurements (a = b = 3.081 Å, c = 10.085 Å for 4H–SiC, and a = b = c = 4.236 Å
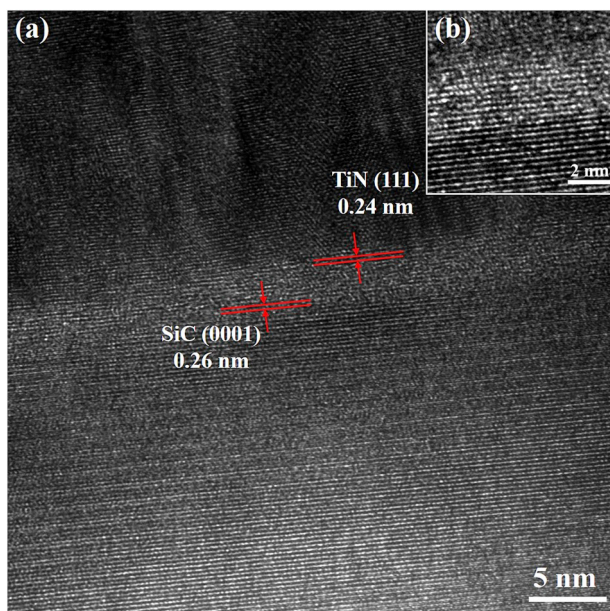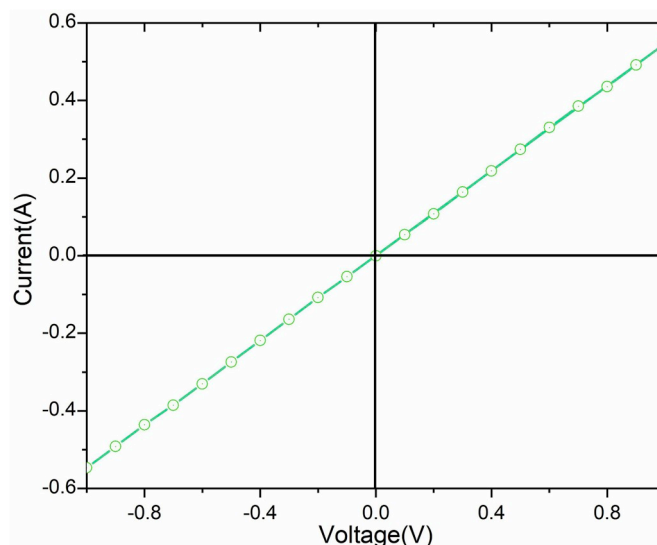
Fig. 3. (a) HRTEM image of TiN/SiC interface, where inset (b) shows the lattice fringes of the interface. Typical crystal planes (111) of TiN and (0001) of 4H–SiC are also shown in the image.
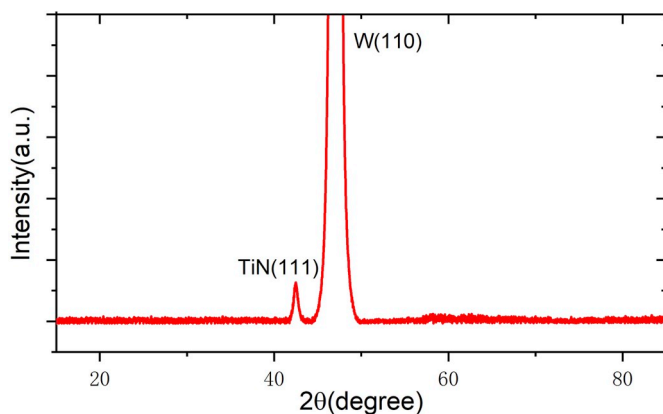
Fig. 4. XRD patterns of W/TiN/SiC systems.

Fig. 5. I–V characteristics of W/TiN/SiC contact.

for TiN) with minor errors of less than 2%. The computed band structures of 4H–SiC are shown in Fig. 6a, in which SiC represents a semiconductor property with an indirect band gap of 2.10 eV. The band gap is smaller than the experiment value [1] because of the intrinsic defect of DFT [28], but agrees well with previous calculated values of 2.18 eV reported by Bechstedt et al. [29] and 2.25 eV reported by Wang et al. [26] In contrast, TiN exhibits a metallic property with bands crossing the Fermi level (Fig. 6b), which is also in line with the previous results [25]. The computed electronic partial density of states (PDOS) in Fig. 7 further verifies the electronic structures. It should be noted that the metallic property of TiN is mainly attributed to the overlap of the Ti 3d and N 2p orbitals at the Fermi level, rather than an artificial error caused by a DFT underestimation of the band gap.

We then study the charge behaviors at the 4H–SiC(0001)/TiN(111) interface, as shown in Fig. 8. In principle, electrons tend to transfer from the low work function side to the high work function side after combining [30] (Fig. 8a). In this work, the work function of 4H–SiC(0001) is much larger than that of TiN(111) (Fig. 9), indicating that after combining electrons tend to transfer from TiN to SiC. As shown in Fig. 8b, the electrons heavily accumulate within the interfacial area, which suggests a good electrical conductivity throughout this region. Further calculations on the charge density differences also demonstrate this point, and it is found that ~0.86 e^- will transfer from TiN to SiC for each unit in our slab model.

The Schottky barrier height (SBH) at the 4H–SiC(0001)/TiN(111) interface is then calculated. In general, SBH is determined based on the difference between the semiconductor band edges and the Fermi level of the interface supercell [31,32], and can be written as follows:

$$\Phi = E_{CBM} - E_F \tag{2}$$

In our case, the SBH is computed as 0.03 eV and the band gap nearly vanishes at the interface (Fig. 10), indicating an excellent Ohmic contact of TiN to 4H–SiC. To shed light on the lower SBH, several analytic approaches are employed to theoretically characterize the detailed interfacial charge distribution, bonding nature, and interfacial electronic states. First, we compute the variation in charge density at the interface. As shown in Fig. 11a, the overall charge density of TiN is higher than that of SiC owing to a higher electronegativity of the N element. Compared with the inner layer atoms, the charge density of Si and Ti undergoes a rearrangement at the Si–Ti interface owing to the interfacial polarization effect. We then calculate the charge-density difference [26] to study the mixture of interfacial electronic states, as shown in Fig. 11b. It is evident that electrons are depleted by both the sub-interfacial N layer and the interfacial Si and Ti layers, suggesting that these layers contribute significantly to the interfacial bonding. Furthermore, the charge density difference fluctuates remarkably near the interface, indicating a significant charge transfer between the SiC and TiN slabs. Such a charge polarization effect at the interface can be more visually presented by the two-dimensional charge density and differences, as shown in Fig. 12. One can see clearly that the transferred electrons accumulate at the interface but should still be classified as more electronegative Si ions than as Ti ions, forming a mixed covalent-
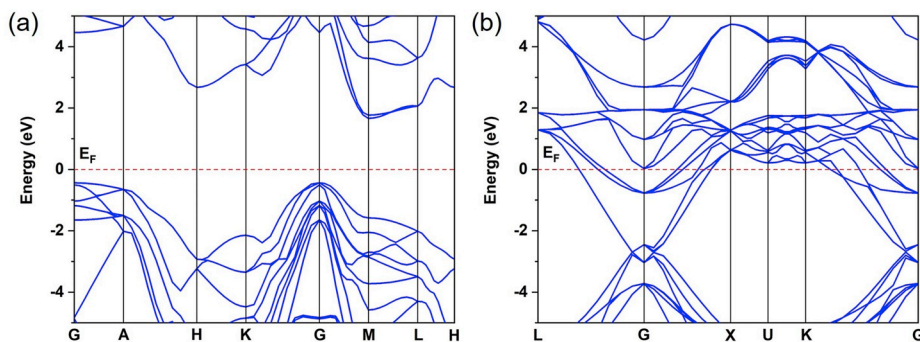
Fig. 6. Energy band structures of (a) 4H–SiC and (b) TiN bulk structures. The horizontal dashed lines denote the Fermi level (E_F).
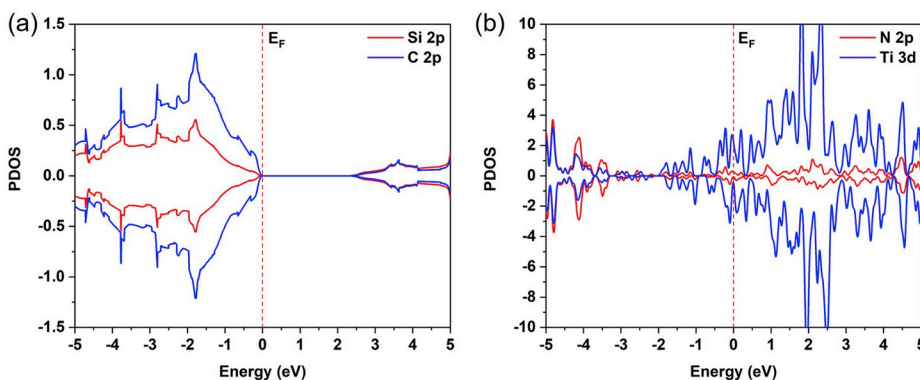

Fig. 7. Electronic PDOS of (a) 4H–SiC and (b) TiN bulk structures. The vertical dashed lines denote the Fermi level (E_F).
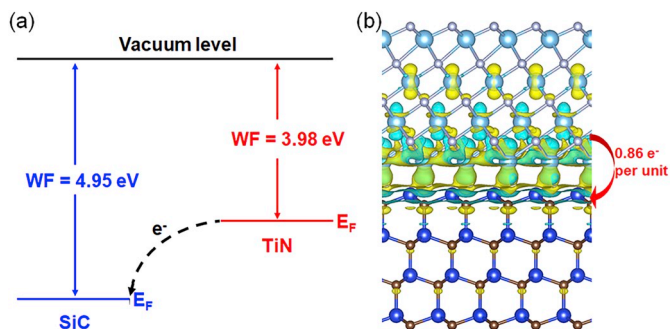

Fig. 8. (a) Schematic illustration of the charge transfer mechanism driven by the difference in work function between 4H–SiC(0001) and TiN(111) surfaces. (b) Charge density differences in 4H–SiC(0001)/TiN(111) interface structure. Yellow and blue bubbles represent electron and hole charge distributions, respectively. (For interpretation of the references to colour in this figure legend, the reader is referred to the Web version of this article.)

Fig. 9. Potential energy surfaces of bare 4H–SiC(0001) (blue) and TiN(111) (red) along the [0001] direction. Work functions are the convergent values of these curves. (For interpretation of the references to colour in this figure legend, the reader is referred to the Web version of this article.)

ionic bonding. In addition, the good current conductivity can also be attributed to a strong coupling of the interfacial electronic states [33], as shown in Fig. 13, exhibiting a very good overlap of all interfacial and sub-interfacial Si 2p, C 2p, Ti 3d, and N 2p orbitals. Moreover, the PDOS of all layers (Fig. 14) suggests that the effect of the interfacial
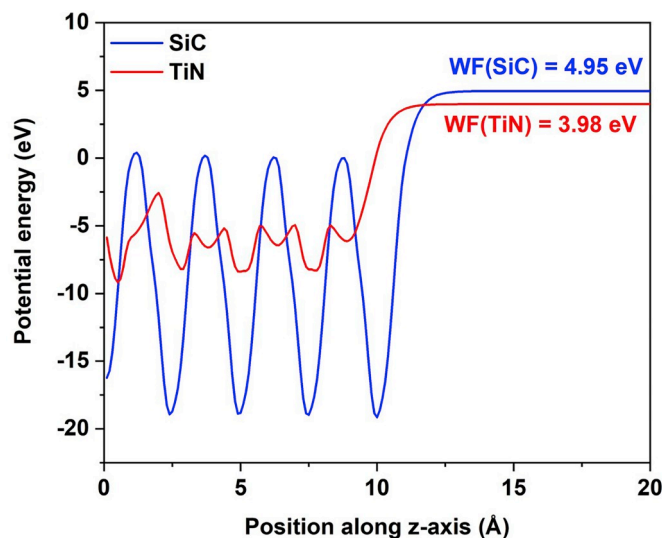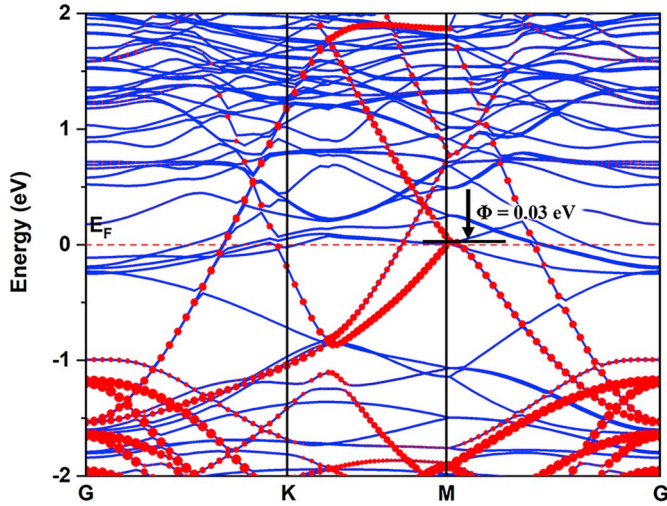
Fig. 10. Band structure of 4H–SiC(0001)/TiN(111) interface. Red dots represent projected bands of SiC. (For interpretation of the references to colour in this figure legend, the reader is referred to the Web version of this article.)

polarization on the electronic states can exist in only a few layers and will eventually return to a bulk PDOS with an increase in the distance from the interface.

5. Conclusion

In summary, the Ohmic contact mechanisms of TiN to 4H–SiC are systematically studied by combining experimental studies with first-principle calculations. HRTEM images illustrate how epitaxially grown TiN atomically bonds to SiC substrates uniformly without any other phases, which is further confirmed by the XRD and HADDF-STEM results. Furthermore, the atomic structure, interfacial charge distribution, bonding nature, and interfacial electronic states of the 4H–SiC(0001)/TiN(111) interface are computed using first-principle calculations. The interfacial charge polarization and strong coupling of the interfacial electronic states can lower the Schottky barrier height to 0.03 eV and thus significantly enhance the quantum electron transport, and are the origins of TiN Ohmic contact to 4H–SiC. The results highlight an important advancement in combining experimental studies with first-principle calculations in an atomic-scale determination of an Ohmic contact interface and present a major step toward addressing the current Ohmic contact issues in SiC devices.
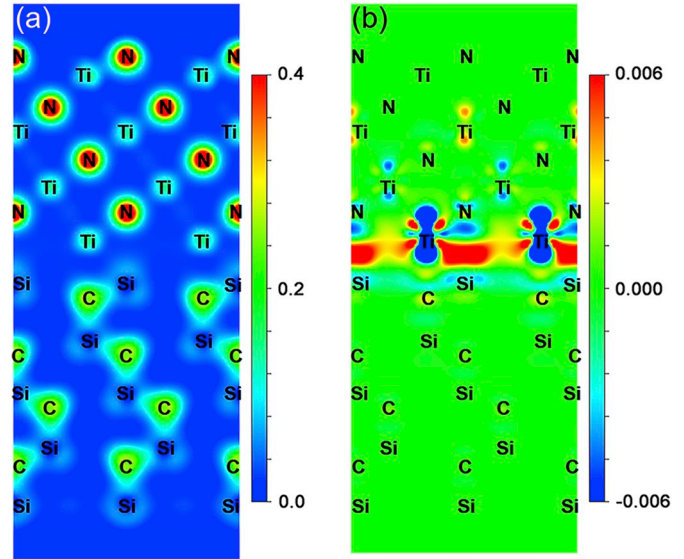

Fig. 12. Contour plot of (a) charge density and (b) its differences along the (11$\bar{2}$0) plane of the 4H–SiC(0001)/TiN(111) interface.
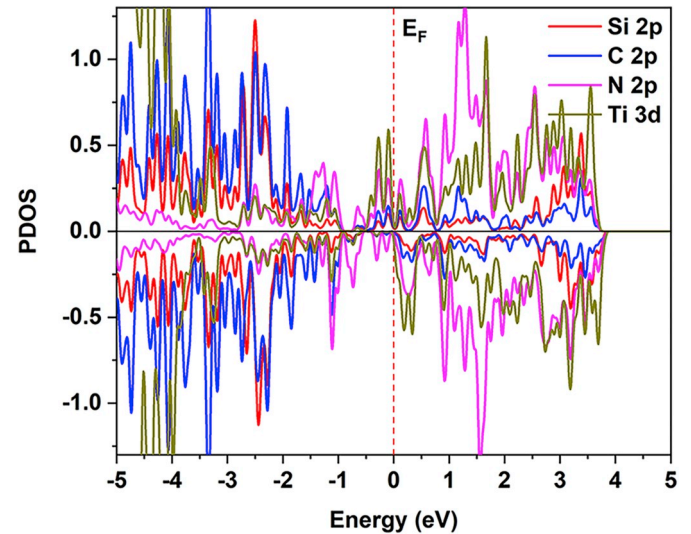

Fig. 13. PDOS of the first Si, C, N, and Ti layers at the 4H–SiC(0001)/TiN(111) interface.
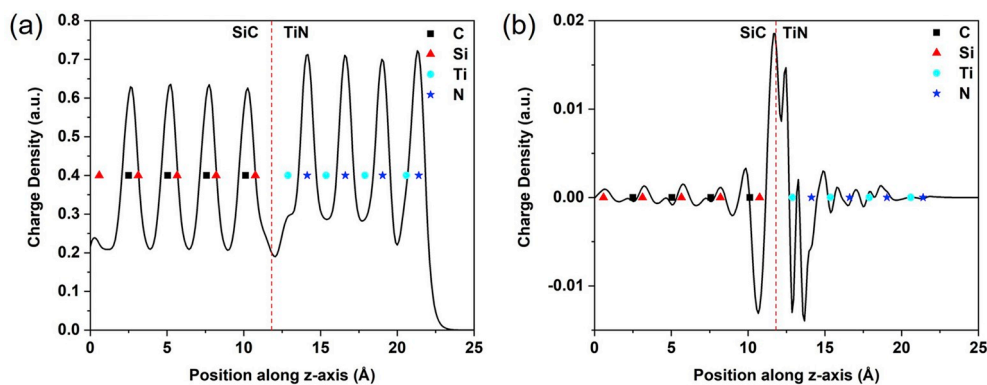

Fig. 11. Computed variation in (a) charge density and (b) differences as a function of distance along the [0001] direction. The interface position is indicated by vertical dashed lines.
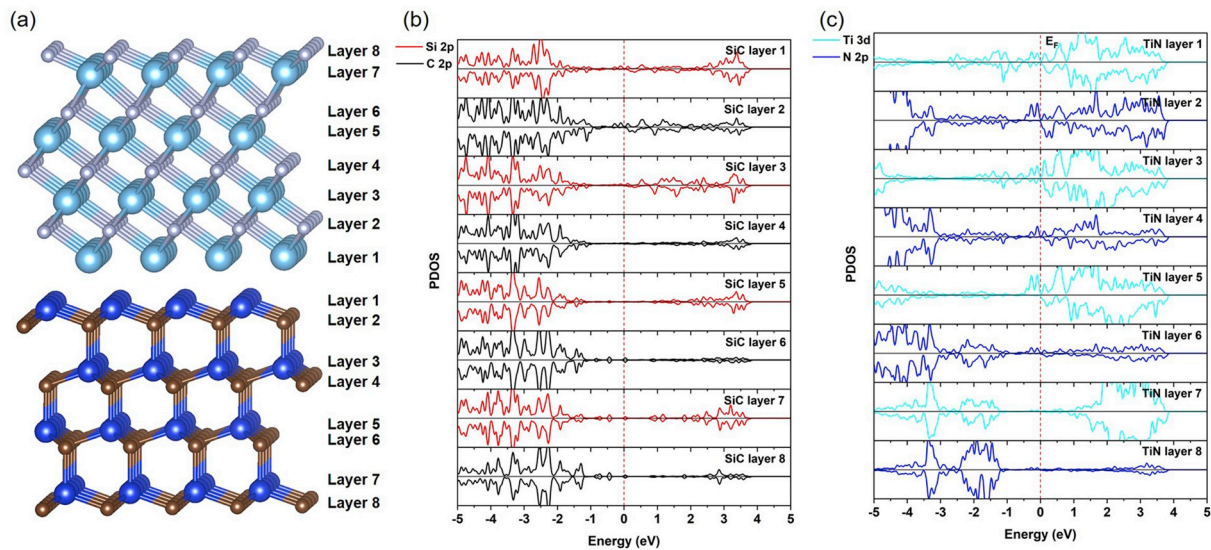
Fig. 14. (a) Atomic structures of SiC(0001)/TiN(111) interface. Computed PDOS of each layer of (b) SiC and (c) TiN in the interface model. The first layer is the atomic layer proximal to the interface. The value of E_F is set to zero and is marked by a vertical dashed line.

Declaration of competing interest

The authors declare that they have no known competing financial interests or personal relationships that could have appeared to influence the work reported in this paper.

Acknowledgements

References

[1] Z. Wang, W. Liu, C. Wang, Recent progress in ohmic contacts to silicon carbide for high-temperature applications, J. Electron. Mater. 45 (2015) 267–284.

[2] F. Roccaforte, P. Fiorenza, G. Greco, R. Lo Nigro, F. Giannazzo, F. Iucolano, M. Saggio, Emerging trends in wide band gap semiconductors (SiC and GaN) technology for power devices, Microelectron. Eng. 187–188 (2018) 66–77.

[3] Y. Liu, J. Guo, E. Zhu, L. Liao, S.J. Lee, M. Ding, I. Shakir, V. Gambin, Y. Huang, X. Duan, Approaching the Schottky-Mott limit in van der Waals metal-semiconductor junctions, Nature 557 (2018) 696–700.

[4] G.-S. Chung, C.-M. Ohn, Ohmic contacts to polycrystalline 3C–SiC films for extreme environment microdevices, Ceram. Int. 34 (2008) 837–840.

[5] B.P. Downey, J.R. Flemish, B.Z. Liu, T.E. Clark, S.E. Mohney, Current-induced degradation of nickel ohmic contacts to SiC, J. Electron. Mater. 38 (2009) 563–568.

[6] B.P. Downey, S.E. Mohney, T.E. Clark, J.R. Flemish, Reliability of aluminum-bearing Ohmic contacts to SiC under high current density, Microelectron. Reliab. 50 (2010) 1967–1972.

[7] S. Tsukimoto, K. Nitta, T. Sakai, M. Moriyama, M. Murakami, Correlation between the electrical properties and the interfacial microstructures of TiAl-based Ohmic contacts to p-type 4H-SiC, J. Electron. Mater. 33 (2004) 460–466.

[8] E. Kurimoto, H. Harima, T. Toda, M. Sawada, M. Iwami, S. Nakashima, Raman study on the Ni/SiC interface reaction, J. Appl. Phys. 91 (2002) 10215–10217.

[9] B. Barda, P. Macháč, M. Hubičková, Ti and Ti/Sb Ohmic contacts on n-type 6H–SiC, Microelectron. Eng. 85 (2008) 2022–2024.

[10] S.Y. Han, K.H. Kim, J.K. Kim, H.W. Jang, K.H. Lee, N.-K. Kim, E.D. Kim, J.-L. Lee, Ohmic contact formation mechanism of Ni on n-type 4H–SiC, Appl. Phys. Lett. 79 (2001) 1816–1818.

[11] J. Crofton, L. Beyer, J. Williams, E. Luckowski, S. Mohney, J. Delucca, Titanium and aluminum-titanium Ohmic contacts to p-type SiC, Solid State Electron. 41 (1997) 1725–1729.

[12] L.M. Porter, R.F. Davis, A critical review of Ohmic and rectifying contacts for silicon carbide, Mater. Sci. Eng. B 34 (1995) 83–105.

[13] C.-T. Lee, Y.-J. Lin, C.-H. Lin, Non alloyed Ohmic mechanism of TiN interfacial layer in Ti/Al contacts to (NH4)2Sx-treated n-type GaN layers, J. Appl. Phys. 92 (2002) 3825–3829.

[14] L. Hultman, H. Ljungcrantz, C. Hallin, E. Janzén, J.E. Sundgren, B. Pécz, L.R. Wallenberg, Growth and electronic properties of epitaxial TiN thin films on 3C-SiC(001) and 6H-SiC(0001) substrates by reactive magnetron sputtering, J. Mater. Res. 11 (2011) 2458–2462.

[15] A.A. Iliadis, S.N. Andronescu, K. Edinger, J.H. Orloff, R.D. Vispute, V. Talyansky, R.P. Sharma, T. Venkatesan, M.C. Wood, K.A. Jones, Ohmic contacts to p-6H–SiC using focused ion-beam surface-modification and pulsed laser epitaxial TiN deposition, Appl. Phys. Lett. 73 (1998) 3545–3547.

[16] B. Pecz, Contact formation in SiC devices, Appl. Surf. Sci. 184 (2001) 287–294.

[17] S. DelaCruz, Z. Wang, P. Cheng, C. Carraro, R. Maboudian, TiN diffusion barrier for stable W/SiC(0001) interfaces in inert ambient at high temperature, Thin Solid Films 670 (2019) 54–59.

[18] R.C. Glass, L.M. Spellman, S. Tanaka, R.F. Davis, Chemical and structural analyses of the titanium nitride/alpha (6H)-silicon carbide interface, J. Vac. Sci. Technol. A 10 (1992) 1625–1630.

[19] G. Kresse, J. Furthmüller, Self-interaction correction to density functional approximation for many electron systems, Phys. Rev. B 54 (1996) 11169.

[20] P.E. Blöchl, Projector augmented-wave method, Phys. Rev. B 50 (1994) 17953.

[21] J.P. Perdew, K. Burke, M. Ernzerhof, Generalized gradient approximation made simple, Phys. Rev. Lett. 77 (1996) 3865.

[22] S. Dudarev, G. Botton, S. Savrasov, C. Humphreys, A. Sutton, Electron-energy-loss spectra and the structural stability of nickel oxide: an LSDA + U study, Phys. Rev. B 57 (1998) 1505.

[23] Y. Liu, Q. Zhu, X. Li, G. Zhang, Y. Liu, S. Tang, E. Sharman, J. Jiang, Y. Luo, Combining high photocatalytic activity and stability via subsurface defects in TiO2, J. Phys. Chem. C 122 (2018) 17221–17227.

[24] W. Tang, E. Sanville, G. Henkelman, A grid-based Bader analysis algorithm without lattice bias, J. Phys. Condens. Matter 21 (2009) 084204.

[25] A. Seifitokaldani, O. Savadogo, M. Perrier, Density functional theory (DFT) computation of the oxygen reduction reaction (ORR) on titanium nitride (TiN) surface, Electrochim. Acta 141 (2014) 25–32.

[26] Z. Wang, S. Tsukimoto, M. Saito, Y. Ikuhara, SiC/Ti3SiC2 interface: atomic structure, energetics, and bonding, Phys. Rev. B 79 (2009).

[27] S.-S. Yang, Y.-R. Lin, S.-T. Wu, Room temperature epitaxial growth of TiN on SiC, Surf. Coat. Technol. 201 (2007) 4850–4854.

[28] M.S. Hybertsen, S.G. Louie, Electron correlation in semiconductors and insulators: band gaps and quasiparticle energies, Phys. Rev. B 34 (1986) 5390.

[29] P. Käckell, B. Wenzien, F. Bechstedt, Electronic properties of cubic and hexagonal SiC polytypes from ab initio calculations, Phys. Rev. B 50 (1994) 10761.

[30] X. Wang, X. Jiang, E. Sharman, L. Yang, X. Li, G. Zhang, J. Zhao, Y. Luo, J. Jiang, Isolating hydrogen from oxygen in photocatalytic water splitting with a carbon-quantum-dot/carbon-nitride hybrid, J. Mater. Chem. 7 (2019) 6143–6148.

[31] K. Nagao, J. Neaton, N. Ashcroft, First-principles study of adhesion at C u/SiO2 interfaces, Phys. Rev. B 68 (2003) 125403.

[32] Y. Liu, P. Stradins, S.-H. Wei, Van der Waals metal-semiconductor junction: weak Fermi level pinning enables effective tuning of Schottky barrier, Sci. Adv. 2 (2016) e1600069.

[33] Y. Liu, H. Xiao, W.A. Goddard, Schottky-Barrier-Free contacts with two-dimensional semiconductors by surface-engineered MXenes, J. Am. Chem. Soc. 138 (2016) 15853–15856.